**Proceedings of the ASME 2021**
**15th International Conference on Energy Sustainability**
**ES2021**
**June 16-18, 2021, Virtual, Online**

SAND2021-4153C

**ES2021-63066**

# TERRESTRIAL HEAT REPOSITORY FOR MONTHS OF STORAGE (THERMS): A NOVEL RADIAL THERMOCLINE SYSTEM

**Clifford K. Ho[1] and Walter Gerstle[2]**
[1]Sandia National Laboratories, Albuquerque, NM, USA
[2]CSolPower, LLC, Albuquerque, NM, USA

## ABSTRACT

*This paper describes a terrestrial thermocline storage system comprised of inexpensive rock, gravel, and/or sand-like materials to store high-temperature heat for days to months. The present system seeks to overcome past challenges of thermocline storage (cost and performance) by utilizing a confined radial-based thermocline storage system that can better control the flow and temperature distribution in a bed of porous materials with one or more layers or zones of different particle sizes, materials, and injection/extraction wells. Air is used as the heat-transfer fluid, and the storage bed can be heated or "trickle charged" by flowing hot air through multiple wells during periods of low electricity demand using electrical heating or heat from a solar thermal plant. This terrestrial-based storage system can provide low-cost, large-capacity energy storage for both high- (~400-800°C) and low- (~100-400°C) temperature applications. Bench-scale experiments were conducted, and computational fluid dynamics (CFD) simulations were performed to verify models and improve understanding of relevant features and processes that impact the performance of the radial thermocline storage system. Sensitivity studies were performed using the CFD model to investigate the impact of the air flow rate, porosity, particle thermal conductivity, and air-to-particle heat-transfer coefficient on temperature profiles. A preliminary technoeconomic analysis was also performed to estimate the levelized cost of storage for different storage durations and discharging scenarios.*

Keywords: THERMS, thermal storage, thermocline, CFD

## NOMENCLATURE

| | |
|---|---|
| CFD | Computational fluid dynamics |
| CSP | Concentrating solar power |
| $d_p$ | Particle size (m) |
| h | Heat transfer coefficient (W/m$^2$-K) |
| $k_f$ | Fluid thermal conductivity (W/m-K) |
| LCOS | Levelized cost of storage ($/kWh$_e$) |
| Nu | Nusselt number |
| Re | Reynolds number |
| u | Velocity (m/s) |
| ν | Air kinematic viscosity (m$^2$/s) |

## 1. INTRODUCTION

Thermal energy storage has been identified as one of the cheapest means of providing large-capacity (≥~1 GWh), long-duration (≥~10 hrs) energy storage to accommodate increasing amounts of intermittent renewable energy on the grid [2, 3]. Current large-capacity thermal-energy storage systems utilize molten salt in concentrating solar power systems [4, 5]. These molten-salt systems suffer from freezing (molten salt freezes at 200 – 300 °C), leaking, tank stresses that can lead to damage, and decomposition of the molten salt at temperatures above 600 °C [6].

Rock-based thermocline storage systems have been tested and modeled as a means to lower the costs of energy storage [7-11]. Most recently, Siemens Gamesa has piloted a 130 MWh rock-bed storage system using air as the heat transfer fluid [12]. In these past thermocline systems, the heat-transfer fluid flows through the packed bed along the axial direction (i.e., for a cylindrical tank, the fluid flows along the axis of the cylinder). These axial-flow thermoclines suffer from an unstable interface between the hot and cold fluids during charging and discharging. The temperature interface becomes diffuse due to flow instabilities, and the premature degradation of the discharging fluid temperature decreases the performance or usability of the power-generation or heat-utilization system.

In contrast to axial-based thermocline storage systems, radial-based thermoclines have been demonstrated and modeled as a means to yield lower costs and more reliable performance [13]. Stellenbosch University has investigated a rock-pile thermal-storage system that consists of rocks dumped onto the ground. A well is placed in the middle of the pile to charge the

Sandia National Laboratories is a multimission laboratory managed and operated by National Technology & Engineering Solutions of Sandia, LLC, a wholly owned subsidiary of Honeywell International Inc., for the U.S. Department of Energy's National Nuclear Security Administration under contract DE-NA0003525

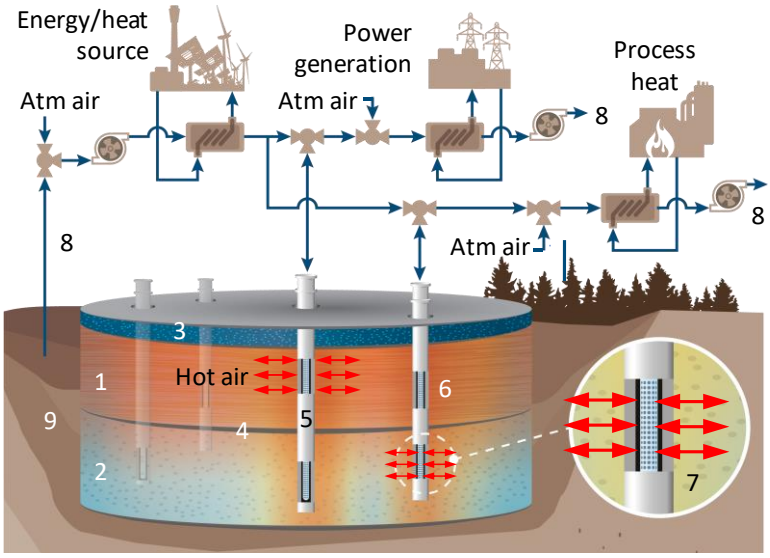


1. Porous storage layer: E.g., gravel, rock, sand, lava rock, bauxite, sintered bauxite
2. Same as 1 (alternate materials)
3. Low permeability cap layer: E.g., clay, sand, recycled glass, firebrick, perlite, bauxite
4. Low permeability layer
5. Primary well for high-temperature (400-800 C) charging/discharging
6. Auxiliary wells for trickle charge and low temperature discharge (100-400 C)
7. Adjustable well liner to control flow in desired layers
8. Optional reuse of warm air
9. Annulus with filler to induce radial flow

**Figure 1. THERMS™ conceptual design for 10–100 GWh of thermal energy storage [1].**

bed of rocks with hot air or to discharge the heat from the bed of rocks when thermal energy is needed. This system can be constructed very cheaply, but it suffers from buoyancy-induced flow and mixing within the rock pile, which degrades the temperatures and subsequent performance of the power-generating or heat-utilization systems. More recently, Trevisan et al. [14, 15] have also modeled and tested bench-scale radial thermocline systems that resulted in promising performance metrics, but large-scale radial thermocline systems were not evaluated.

This work evaluates a unique terrestrial thermocline storage system comprised of inexpensive rock, gravel, and/or sand-like materials to store high-temperature heat for days to months. The remainder of this paper provides a description of the heat-repository design, a high-level technoeconomic analysis, and bench-scale modeling and testing of a representative system.

## 2. SYSTEM OVERVIEW

Figure 1 illustrates the general design of our proposed Thermal Heat Repository for Months of Storage (THERMS™) [1]. Hot air is obtained from a heat source that can be an electrical heater, concentrating solar power, or waste heat. The hot air is injected using blowers through a primary well into porous layers and any number of additional layers that can be comprised of gravel, rock, sand, sintered bauxite, or other porous materials. The type and size of material can be varied to optimize the permeability/flow of the layers while minimizing buoyancy. Different layers can be designed to maintain different temperatures for different applications such as power generation or process heating. Auxiliary wells arranged around the primary well (e.g., in a radial or circumferential pattern) can be used to inject additional energy from the heat source to cooler regions of the storage bed. The arrangement of the wells can borrow from oil/gas, groundwater, and geothermal industries to optimize the injection and withdrawal of energy flows. The storage bed can be cylindrical or conical.

When energy is needed, the pumps are used to withdraw air from the primary well for delivery to the power-generating unit or process-heat unit. The auxiliary wells can be used to pull lower temperature air for use in lower-temperature applications such as process heating. The primary and auxiliary wells can be fitted with retractable liners or sleeves to direct the flow of air to and from prescribed layers for controlled heating and temperatures (see inset in Figure 1). Ambient air can be blended with the hot withdrawn air using valves and pumps to regulate and maintain the temperature for use in the power-generating unit or process-heat unit.

A low-permeability cap can be installed on top of the storage repository to mitigate buoyancy effects and heat loss through the top. The cap can be made of clay, rock, sintered bauxite, glass (recycled), firebrick, pearlite, sand, or any other suitable high-temperature material. Capillary barriers that are used to prevent fluid transport, including infiltration of rain water into landfills, can also be implemented at the top of the repository [16-18].

A low-permeability layer can be installed in between layers 1 and 2 (and any additional layers) to mitigate inter-layer buoyancy effects and maintain uniform temperatures in each layer. An annulus around the storage bed can be filled with gravel, refractory material, sintered bauxite, sand, rocks, boulders, or lined with mesh/screen to enable the radial flow of air from the center to the periphery. Auxiliary wells can be placed in the annulus, as needed, to extract heat and induce airflow.

Advantages of the current system over previous particle-based thermoclines include a radial flow configuration with multiple layers of materials to maintain zones of different temperatures for multiple applications (e.g., electricity production (600 – 800 °C), process heat (100 – 600 °C)). Also, terrestrial-based storage eliminates the need for expensive steel

or nickel-based containment materials. Air is used as the heat-transfer fluid, and the system can be heated or "trickle charged" for long-term storage through multiple wells during periods of low electricity demand from a CSP plant or via direct electrical heating. The multi-well configuration will enable regeneration of zones and extraction of variable-temperature heat, as needed. The radial configuration yields the hottest temperatures within the self-insulated interior core regions of the storage bed, while cooler temperatures are located toward the periphery, minimizing temperature gradients and heat loss to the surrounding earth. The acceleration and convergence of air flow towards the interior during discharge is expected to yield more stable temperature profiles than previous axial thermocline designs for end-use applications.

## 3. MODELING AND ANALYSES

In this study, a high-level technoeconomic analysis and bench-scale testing and modeling were performed. The technoeconomic analysis provided an assessment of current potential costs of a thermal repository (without optimization) and opportunities for cost reduction. Different energy storage discharge scenarios were investigated and compared to a lithium-ion battery storage system. The bench-scale testing and modeling were performed to better understand key parameters and processes that can be used in future design studies to improve performance (e.g., reduce heat losses and pressure drop).

### 3.1. Technoeconomic Analysis

We consider the case where one of three of the 50 $MW_e$ gas-fired steam-generating units at the 150 $MW_e$ Reeves thermoelectric generating station in Albuquerque, New Mexico, is to be retrofitted with THERMS™. We assume, in terms of capital expenditure, that the legacy power plant is cost-free. The only capital expenditure is for the THERMS™ components, materials, and connection (see Appendix). Two storage use-cases are evaluated for comparison purposes: (1) 4-hour discharge, 200 times per year and (2) 168-hour (1-week) discharge, 2 times per year.

For these use-cases, we assume the (unoptimized) THERMS™ design consists of a gravel-based repository 10 m high by ~15 m in radius (for case 1) and 89 m in radius (for case 2) based on energy storage requirements, with 6 m-thick insulating material to limit environmental heat loss to 0.2% per day. A single layer of basalt gravel (6 cm particle diameter) is assumed for the storage layer with a porosity of 0.4, yielding a permeability of 3.6e-6 $m^2$. Hot air from THERMS™ is assumed to provide heating from ~400 – 700 °C.

The levelized cost of storage (LCOS) is defined as follows [19]:

$$LCOS = \frac{\sum (Capital_t + O\&M_t + Fuel_t) \cdot (1+r)^{-t}}{\sum MWh_t \cdot (1+r)^{-t}}$$

where $Capital_t$ = total capital expenditures in year t, $O\&M_t$ = operation and maintenance costs in year $t$, $Fuel_t$ = electrical charging cost in year t, $MWh_t$ = the amount of electricity discharged in MWh in year t, and $(1+r)^{-t}$ = discount factor for year t, and $r$ = discount rate (assumed 8% annually).

We assume a 30-year lifetime for THERMS™ and an electricity cost for charging THERMS™ of $0.03/kWh. The model assumes realistic performance parameters (e.g., thermal-to-electric efficiency = 30% with availability of 90%) and includes conservative assumptions regarding costs for materials, excavation, electric heater, blowers, controls, ducting, land, site improvement, connections, engineering, construction, owner activities, gross receipts tax, financing, labor, and O&M (see Appendix for summary of model parameters). The CAPEX for the construction and installation of the 50 MWe THERMS™ storage and conversion system is $7.04M and $26.11M for the short-duration and long-duration storage scenarios, respectively, and assumed to be spent in year one. The operations and maintenance cost ($O\&M_t$) includes annual labor and repair costs that are ~17% and 5% of the initial capital cost for the short-duration and long-duration scenarios, respectively.

Figure 2 shows the estimated LCOS for both the short-duration and long-duration storage cases with the current assumed baseline configuration and two additional scenarios. The first additional scenario is for an optimized THERMS™ system that includes the following improvements: 1) long-duration storage bin height is increased from 10 m to 30 m, which reduces the radial extent and parasitic pumping requirements, 2) the thermal-to-electric efficiency is increased from 0.3 to 0.5 (advanced or combined power cycles), 3) the O&M labor is reduced from two full-time staff to one (automation, controls), and 4) the annual repair costs are reduced from $1M/yr to $0.1M/yr based on improvements to reliability. The second additional scenario includes all of the benefits of the optimized system plus an assumed reduction in electricity costs from $0.03/$kWh_e$ to $0.01/$kWh_e$ assuming that curtailed electricity can be combined with low-cost renewable energy generation for charging THERMS™.

The resulting LCOS ranges from $0.037/$kWh_e$ – $0.146/$kWh_e$ for the short-duration storage scenario, and from $0.129/$kWh_e$ – $0.466/$kWh_e$ for the long-duration scenario. The long-duration LCOS is significantly more expensive because of the reduced generation of electricity from storage (only 2 weeks of discharge per year compared to 4 hours x 200 discharges = 4.8 weeks). For a combination of short-duration and long-duration discharges, the calculated THERMS™ LCOS ranges from $0.053 – $0.21/$kWh_e$.

For lithium-ion battery storage systems, the National Rural Electric Cooperative Association estimated a range of battery system costs between $0.108/$kWh_e$ - $0.471/$kWh_e$, depending upon specific use-cases, for short-duration storage [20]. For the long-duration storage scenario, assuming equivalent costs and financing parameters as the THERMS™ assessment, we estimate LCOS to be ~$14/$kWh_e$, which is extremely high because of the large capital cost (assuming ~$200/$kWh_e$ CAPEX for the entire battery system), limited lifetime (~10 years), and limited discharge of stored electricity for the long-duration scenario (two weeks per year).

Therefore, the LCOS of THERMS™ is expected to be orders of magnitude less expensive than that of battery storage for long-duration scenarios and comparable in costs for short-duration scenarios. Thermal energy storage that is charged with curtailed renewable energy is highly advantageous and can directly supply heat to legacy gas- and coal fired power plants, while also providing industrial and district heating using waste heat, and additional value not considered in this analysis.

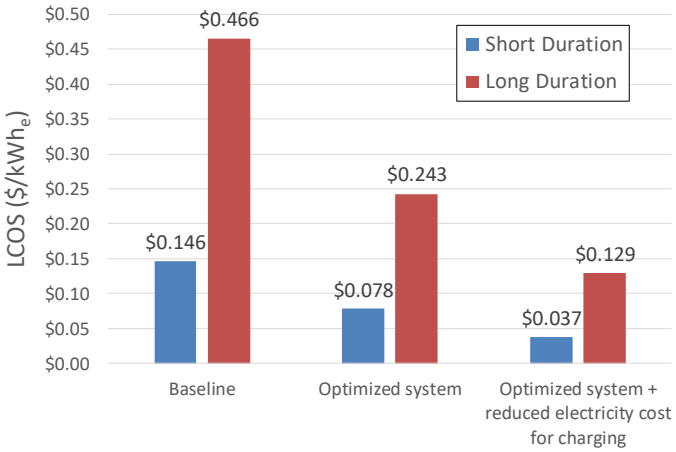


**Figure 2. Estimated LCOS for short-duration (4 hrs discharge, 200 discharges/year) and long-duration (168 hrs discharge (1 week), 2 discharges/year) storage scenarios.**

### 3.2. Bench-Scale Testing and Modeling

The previous technoeconomic analysis made assumptions regarding the performance and heat loss of the thermal repository. In order to improve and optimize the design of the THERMS™ system, more detailed models and understanding of the flow and heat-transfer processes are required. Therefore, small-scale tests and computational fluid dynamics (CFD) modeling were performed to develop a better understanding of the key processes and to build confidence in the models.

#### 3.2.1. Bench-Scale Testing

In the spirit of developing simple, low-cost storage solutions, a "backyard" radial bench-scale thermocline test was performed using common household materials. The tests consisted of a 3" (7.6 cm) thick layer of air-dried pea gravel sandwiched between two plastic potting saucers that were 17" (43 cm) diameter on the bottom and 15" (38 cm) diameter on the top. Fiberglass insulation (¾" (1.9 cm)) thick was placed on top of the bottom saucer and covered with a polyethylene plastic liner. The pea gravel was placed on top of the plastic liner, followed by another polyethylene liner, another layer of ¾" fiberglass insulation, and finally the top saucer (Figure 3). A beer can with its top removed, and perforated within the gravel layer, was used as the central air duct through which hot air was blown using a hair drier, as shown in Figure 4.

Temperatures were measured using cooking thermometers. All meat thermometers were evaluated together at ambient temperature and recorded ambient temperatures to within +/- 2 °C of each other. The ability to read each thermometer using the analog display was +/- 1°C. The total estimated error of the thermometers was therefore assumed to be +/- 3°C.

A large ~60-gallon (0.227 $m^3$) trash bag shown in Figure 5 was used to measure the flow rate of air from the hair dryer. With the hair drier on low speed, it took about 35 seconds to fill the trash bag through the 3"-thick gravel bed, resulting in a flow rate of ~0.229 $ft^3/s$ (~8e-4 $m^3/s$).

**Figure 3. Sequence of photos showing the assembly of the bench-scale radial-thermocline test.**

**Figure 4. Assembled bench-scale test with thermometers and hair dryer in place.**

Figure 6 shows the results of a test in which the hair dryer was turned on for ~60 minutes, and then the system was allowed to cool under ambient conditions. Temperatures within the gravel bed rose rapidly as the hot air flowed through the system. The regions near the hair dryer at radial distances of 5" (~13 cm) or less achieved a peak temperature of ~70 °C. Further away from the center, the temperatures reached a lower peak temperature due to heat loss from the system. After the hair dryer was turned off, the system began to cool caused by conduction through the gravel and insulation, and convection to the environment. These

tests were used to verify CFD models and understand key processes for future design studies.

**Figure 5. Measurement of airflow using a trash bag.**

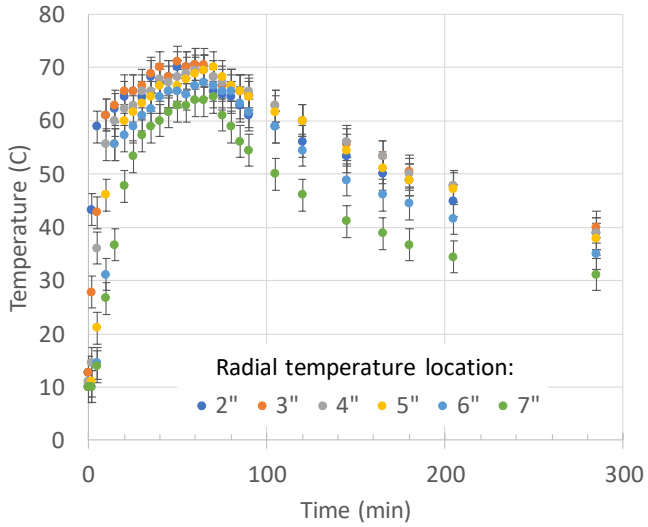


**Figure 6. Measured temperatures as a function of time in bench-scale test at six locations: 2" (5.08 cm), 3" (7.62 cm), 4" (10.2 cm), 5" (12.7 cm), 6" (15.2 cm), and 7" (17.8 cm)**

### 3.2.2. CFD Modeling of Bench-Scale Tests

Solidworks Flow Simulation is a commercial software package [21] that was used to perform the CFD simulations in this study. Flow Simulation solves the conservation of mass, momentum, energy, and species equations using a discrete numerical finite-volume approach. For turbulent flows, Flow Simulation solves the Favre-Averaged Navier-Stokes (FANS) equations. FANS uses a mass-weighted time-averaging scheme, which can avoid complications associated with the Reynolds Averaged Navier Stokes (RANS) solutions for compressible flows (for incompressible low-Mach flow conditions, FANS and RANS solutions are similar). Meshing is performed using a combination of hexahedral and polyhedral elements, which accommodate curved boundaries between phases or materials. Additional details of the numerical formulations, conservation equations, constitutive relations, meshing, and solution techniques can be found in the technical reference manual [21].

Figure 7 shows the model domain of the simulated bench-scale test. A $1/8^{th}$ symmetry section was used to simplify the CFD simulation, and a mesh resolution study was performed to determine grid independence on the simulated temperature profiles. Buoyancy was neglected, and the gravel bed was modeled as a porous medium in Flow Simulation. The properties of the pea gravel and parameters used in the model are summarized in Table 1.

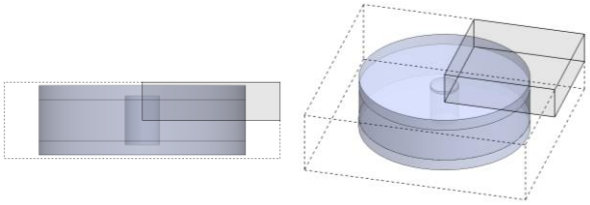

**Figure 7. Two views of the CFD model geometry. Symmetry is employed so that only 1/8 of the model domain is simulated. Initial and boundary conditions taken from experiments.**

**Table 1. Summary of model parameters for bench-scale test.**

| Parameter | Value | Notes |
|---|---|---|
| Avg particle diameter, $d_p$ (m) | 0.00635 | Measured |
| Average pore size (m) | 0.0029 | Estimated based on particle size [22, 23] |
| Porosity | 0.5 | Assumed |
| Thermal conductivity of pea gravel (W/m-K) | 2.79 | Granite [24]. Multiplied by solid volume fraction (1-porosity) to get effective thermal conductivity of bed. |
| Density of pea gravel (kg/m$^3$) | 2630 | Granite [24]. Multiplied by solid volume fraction (1-porosity) to get effective thermal conductivity of bed. |
| Specific heat of pea gravel (J/kg-K) | 775 | Granite [24] |
| Thermal conductivity of fiberglass (W/m-K) | 0.038 | [24]. Function of temperature. |
| Density of fiberglass (kg/m$^3$) | 24 | [24] |
| Specific heat of fiberglass (J/kg-K) | 835 | [24] |
| Air flow rate (m$^3$/s) | 8e-4 | Measured |
| Air velocity (m/s) | ~0.1 – 1 | Based on flow rate, porosity, and radial distance |
| Temperature of hot air (°C) | 71 | Measured |
| Ambient temperature (°C) | 10 - 20 | Measured (variable with time) |
| Air properties | Variable | Determined in CFD model |

The porous medium adds a resistance to flow, and the permeability and pressure drop are related by Darcy's law. The calculated permeability in Flow Simulation is a function of the air kinematic viscosity, average pore size, and porosity.

The solid-fluid heat transfer coefficient has been empirically determined by Wu and Hwang [25] and the following Nusselt number correlation was provided for porosities ~0.4:

$$Nu = 0.32\,\mathrm{Re}^{0.59} \tag{1}$$

where

$$\mathrm{Re} = \frac{u d_p}{\nu} \tag{2}$$

The solid-fluid heat-transfer coefficient was determined from the Nusselt number as follows:

$$h = \frac{Nu\, k_f}{d_p} \tag{3}$$

The heat transfer coefficient between the confining saucers and the external environment was assumed to be 10 W/m$^2$-K to account for buoyancy and convective heat transfer.

Figure 8 shows the transient simulation results of the bench-scale test described in Section 3.2.1. During heating, the flow of hot air through the porous medium increases the temperature with time. After 60 minutes of heating, the system was allowed to cool, and at 280 minutes, the temperature has decreased due to conduction through the porous medium and insulation, and convection to the environment. In the simulations, the measured ambient temperatures were used as the initial and boundary condition.

Figure 9 shows the simulated transient temperatures along with the measured temperatures at six locations. Although differences exist due to uncertainties in boundary conditions (e.g., heat loss), hot-air flow rate and temperatures, and a simplified model geometry, the general trend in measured temperatures is matched by the CFD simulations. Future modeling will evaluate the performance of the radial thermocline and ways to optimize the system design.

**Sensitivity Studies**

A number of sensitivity studies were performed using the CFD model to investigate the impact of various parameters and processes. Decreasing the air flow rate reduces the velocity, which had a significant impact on the heating rate and transient temperature profile in the porous medium, especially at larger radial distances. At the furthest radial temperature reading of 18 cm (7") from the center, the measured temperature was nearly 50% lower when the flow rate was reduced by half.

A larger simulated porosity decreased the bulk density and heat capacitance of the porous medium (the intrinsic density of the solid is multiplied by the solid volume fraction (1 – porosity). As a result, less heat was absorbed by the solid medium, and the temperatures were relatively lower than with a lower simulated porosity.

The solid thermal conductivity influenced the radial dissipation of heat through the porous medium. A larger thermal conductivity reduced the rate of temperature increase throughout the gravel as the energy was conducted away more rapidly. The increased dissipation also resulted in increased temperatures at greater radial distances initially, but after ~20 min, the simulated temperatures were generally lower.

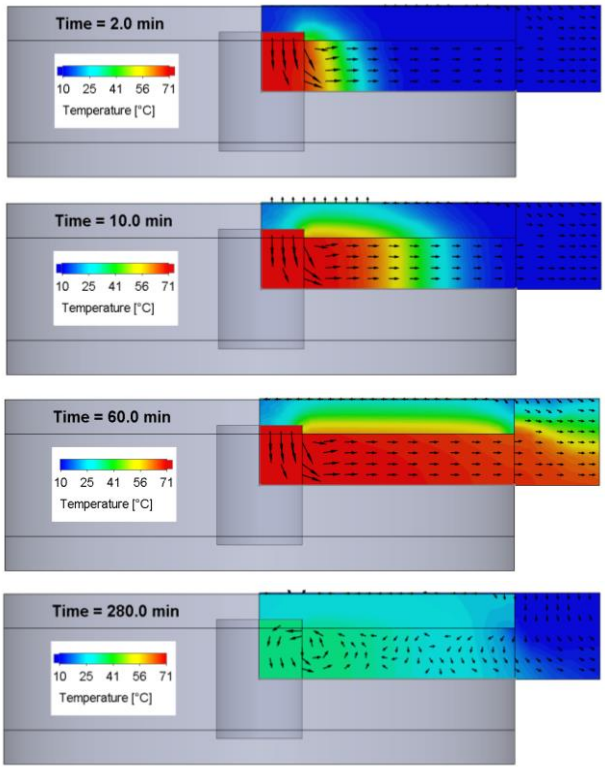


**Figure 8. Simulated transient temperature contours at 2, 10, 60, and 280 min of the bench-scale test. Hot-air flow occurred for ~60 min.**

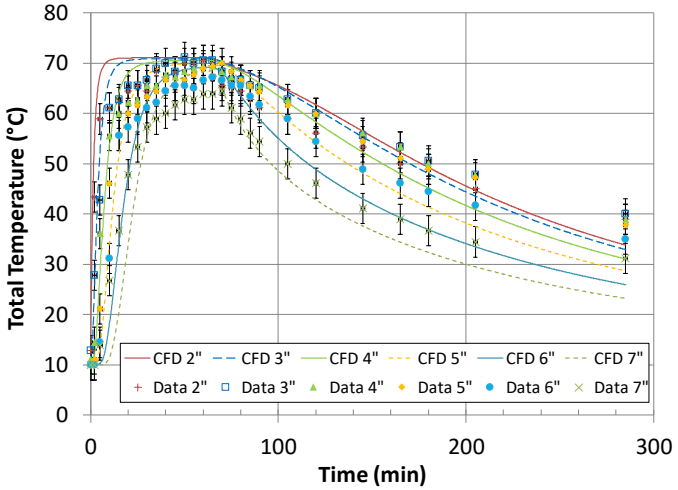


**Figure 9. Simulated and measured temperatures as a function of time at six locations recorded during the experiment.**

The solid-fluid heat-transfer coefficient also impacted the transient temperature profiles when the value was prescribed to be on the order of 10 $W/m^2$-K or less. With low solid-fluid heat-transfer coefficients, less heat-exchange occurred between the flowing air and the solid matrix, reducing the thermocline effect and diffusing the temperature profile spatially. Sensitivity studies also showed that the simulated transient temperature profiles were insensitive to changes in the solid-fluid heat-transfer coefficient above ~$10^2$. It should be noted that Wu and Hwang [25] experimentally derived values for the solid-fluid heat-transfer coefficient that were on the order of ~10 - 100 for the range of fluid pore velocities simulated in this study (~0.1 – 1 m/s). In addition, when using the empirical solid-fluid heat-transfer coefficient, the simulated difference in temperature between the air and solid within the porous medium was as high as 6 °C within 2 minutes of initial heating, but as the porous medium continued to heat, the difference in temperature between the solid and air was simulated to be less than ~1 – 2 °C throughout the domain.

## 4. CONCLUSIONS

A radial terrestrial heat repository for months of storage (THERMS™) was introduced as a means to provide large-capacity, long-duration storage for electrical-grid and process-heat applications. A technoeconomic analysis was performed that showed the LCOS of THERMS™ ranged from ~$0.04/$kWh_e$ – $0.15/$kWh_e$ for short-duration storage applications and from ~$0.13/$kWh_e$ – $0.47/$kWh_e$ for long-duration storage applications for a 50 $MW_e$ thermoelectric power plant. Bench-scale tests and CFD modeling were performed to develop proof-of-concept testing, better understand salient processes and features, and build confidence in the models. Results showed reasonable comparison between the CFD model results and measured transient temperatures. Future work will improve and optimize designs of the radial thermocline system using CFD modeling with validation from pilot-scale tests employing both charging and discharging scenarios.

## ACKNOWLEDGMENTS

Thanks to Henk Laubscher and an anonymous reviewer for their reviews of this work (and the anonymous reviewer's appreciation of La Cumbre beer). This work was funded in part by the NM Small Business Assistance Program. Sandia National Laboratories is a multimission laboratory managed and operated by National Technology and Engineering Solutions of Sandia, LLC., a wholly owned subsidiary of Honeywell International, Inc., for the U.S. Department of Energy's National Nuclear Security Administration under contract DE-NA0003525.

## REFERENCES

[1] Ho, C.K., H.F. Laubscher, and P. Gauché, United States Patent Application 17023550, Radial Particle-Based Terrestrial Thermocline for High Temperature Thermal Storage, Sandia National Laboratories, 9/17/20, SD15304.0/S165409.

[2] Forsberg, C., P. Sabharwall, and H.D. Gougar, 2019, Heat Storage Coupled to Generation IV Reactors for Variable Electricity from Baseload Reactors: Changing Markets, Technology, Nuclear-Renewables Integration and Synergisms with Solar Thermal Power Systems, Massachusetts Institute of Technology, Idaho National Laboratory, Exelon, MIT-ANO-TR-185, INL/EXT-19-54909, Cabridge, MA.

[3] Branz, H.M., W. Regan, K.J. Gerst, J.B. Borak, and E.A. Santori, 2015, Hybrid solar converters for maximum exergy and inexpensive dispatchable electricity, *Energy & Environmental Science*, **8**(11), p. 3083-3091.

[4] Gil, A., M. Medrano, I. Martorell, A. Lazaro, P. Dolado, B. Zalba, and L.F. Cabeza, 2010, State of the art on high temperature thermal energy storage for power generation. Part 1-Concepts, materials and modellization, *Renewable & Sustainable Energy Reviews*, **14**(1), p. 31-55.

[5] Siegel, N.P., 2012, Thermal energy storage for solar power production, *Wiley Interdisciplinary Reviews-Energy and Environment*, **1**(2), p. 119-131.

[6] Bradshaw, R.W. and D.E. Meeker, 1990, High-Temperature Stability of Ternary Nitrate Molten-Salts for Solar Thermal-Energy Systems, *Solar Energy Materials*, **21**(1), p. 51-60.

[7] Yang, Z. and S.V. Garimella, 2010, Molten-salt thermal energy storage in thermoclines under different environmental boundary conditions, *Applied Energy*, **87**(11), p. 3322-3329.

[8] Flueckiger, S.M., Z. Yang, and S.V. Garimella, 2012, Thermomechanical Simulation of the Solar One Thermocline Storage Tank, *Journal of Solar Energy Engineering-Transactions of the Asme*, **134**(4).

[9] Zanganeh, G., A. Pedretti, S.A. Zavattoni, M.C. Barbato, A. Haselbacher, and A. Steinfeld, 2014, Design of a 100 MWh(th) packed-bed thermal energy storage, *Proceedings of the Solarpaces 2013 International Conference*, **49**, p. 1071-1077.

[10] Zanganeh, G., A. Pedretti, A. Haselbacher, and A. Steinfeld, 2015, Design of packed bed thermal energy storage systems for high-temperature industrial process heat, *Applied Energy*, **137**, p. 812-822.

[11] Zavattoni, S.A., M.C. Barbato, A. Pedretti, and G. Zanganeh, 2015, Single-tank TES system - Transient evaluation of thermal stratification according to the second-law of thermodynamics, *International Conference on Concentrating Solar Power and Chemical Energy Systems, Solarpaces 2014*, **69**, p. 1068-1077.

[12] Siemens Gamesa. *Electric Thermal Energy Storage*. 2020 [cited 4/18/2020 4/18/2020]; Available from: https://www.siemensgamesa.com/en-int/products-and-services/hybrid-and-storage/thermal-energy-storage-with-etes.

[13] Laubscher, H.F., T.W. von Backstrom, and F. Dinter, 2017, Developing a Cost Effective Rock Bed Thermal Energy Storage System: Design and Modelling, *International Conference on Concentrating Solar Power and Chemical Energy Systems (Solarpaces 2016)*, **1850**.

[14] Trevisan, S., R. Guedez, H. Bouzekri, and B. Laumert, 2019, Initial Design of a Radial-Flow High Temperature Thermal Energy Storage Concept for Air-Driven CSP Systems, *Solarpaces 2018: International Conference on Concentrating Solar Power and Chemical Energy Systems*, **2126**.
[15] Trevisan, S., W. Wang, R. Guedez, and B. Laumert, 2020, *Laboratory Prototype of an Innovative Radial Flow Packed Bed Thermal Energy Storage*, in *Solarpaces 2020: International Conference on Concentrating Solar Power and Chemical Energy Systems*,
[16] Ho, C.K., T.J. Goering, J.L. Peace, and M.L. Miller, 2005, Probabilistic Performance-Assessment Modeling of the Mixed Waste Landfill at Sandia National Laboratories, SAND2005-6888, Sandia National Laboratories, Albuquerque, NM.
[17] Ho, C.K., 2008, Analytical risk-based model of gaseous and liquid-phase radon transport in landfills with radium sources, *Environmental Modelling & Software*, **23**(9), p. 1163-1170.
[18] Ho, C.K., B.W. Arnold, J.R. Cochran, R.Y. Taira, and M.A. Pelton, 2004, A probabilistic model and software tool for evaluating the longterm performance of landfill covers, *Environmental Modelling & Software*, **19**(1), p. 63-88.
[19] Schmidt, O., S. Melchior, A. Hawkes, and I. Staffell, 2019, Projecting the Future Levelized Cost of Electricity Storage Technologies, *Joule*, **3**(1), p. 81-100.
[20] National Rural Electric Cooperative Association, National Rural Utilities Cooperative Finance Corporation, CoBank, and NRTC, 2019, "Battery Energy Storage Overview", 2019 Business & Technology Report, Updated April 2019, https://www.cooperative.com/programs-services/bts/Documents/Reports/Battery-Energy-Storage-Overview-Report-Update-April-2019.pdf,
[21] Dassault Systems, 2019, Technical Reference Solidworks Flow Simulation 2019, www.solidworks.com,
[22] Raffray, A.R. and J.E. Pulsifer, 2003, MERLOT: a model for flow and heat transfer through porous media for high heat flux applications, *Fusion Engineering and Design*, **65**(1), p. 57-76.
[23] Roozbahani, M.M., R. Borela, and J.D. Frost, 2017, Pore Size Distribution in Granular Material Microstructure, *Materials*, **10**(11).
[24] Incropera, F.P., D.P. DeWitt, 1985, *Introduction to Heat Transfer*, John Wiley & Sons, New York.
[25] Wu, C.C. and G.J. Hwang, 1998, Flow and heat transfer characteristics inside packed and fluidized beds, *Journal of Heat Transfer-Transactions of the Asme*, **120**(3), p. 667-673.

## APPENDIX

Table 2 contains a summary of baseline parameters used in the technoeconomic analysis of the use-case in which a 50 $MW_e$ thermoelectric power plant is retrofitted with THERMS™ for two storage scenarios: (1) 4 hours of storage with 200 discharges per year and (2) 168 hours (1 week) of storage with 2 discharges per year.

**Table 2. Summary of baseline parameters for technoeconomic analysis with two storage scenarios: (1) 4 hours of storage with 200 discharges per year and (2) 168 hours (1 week) of storage with 2 discharges per year.**

| Parameter | Units | Case 1 | Case 2 |
|---|---|---|---|
| System Parameters | | | |
| Electrical Discharge Power (plus parasitic pumping power) | MW | 56 | 56 |
| Discharging duration | hours | 4 | 168 |
| Density of basalt rock | kg/m3 | 3000 | 3000 |
| Porosity | - | 0.4 | 0.4 |
| Gravel particle diameter | m | 0.06 | 0.06 |
| Permeability of gravel (Kozeny-Carman) | $m^2$ | 3.6E-06 | 3.6E-06 |
| Heat capacity of basalt gravel | J/(kg-C) | 840 | 840 |
| Thermal conductivity of basalt gravel | W/(m-C) | 1.5 | 1.5 |
| Electrical Storage Capacity | MWh | 224 | 9410 |
| Thermal Storage Capacity | MWh | 747 | 31,400 |
| Total volume of gravel | $m^3$ | 5,926 | 248,889 |
| Required air flow, Q (total, all modules) | $m^3/s$ | 1,810 | 1,810 |
| Required Inner Radius of each Cylindrical Module | m | 1.44 | 1.44 |
| Height of repository | m | 10 | 10 |
| Outer Radius (minimum) | m | 14.75 | 89.17 |
| Inlet air pressure | Pa | 337 | 936 |
| Parasitic Power needed to blow air | MW | 0.61 | 1.69 |
| Number of discharge times per year | times/ year | 200 | 2 |
| Availability | - | 0.90 | 0.90 |
| Total electrical power discharged per charging cycle | MWh/ cycle | 222 | 9,123 |
| Initial Capital Cost | | | |
| Unit cost of basalt gravel | $/$m^3$ | 20 | 20 |
| Unit cost of excavation | $/$m^3$ | 20 | 20 |
| Cost of electric heater and air fan | million $ | 1.00 | 1.00 |
| Cost of controls | million $ | 1.00 | 1.00 |
| Cost of ducting | million $ | 1.00 | 1.00 |
| Cost of land | million $ | 0.00 | 0.00 |

| Parameter | Units | Case 1 | Case 2 |
|---|---|---|---|
| Site improvement cost | million $ | 0.10 | 0.10 |
| Connection to heat recovery steam turbine, etc. | million $ | 2.00 | 2.00 |
| Cost of engineering | million $ | 0.34 | 1.33 |
| Cost of construction contracting | million $ | 0.51 | 1.99 |
| Cost of owner activities | million $ | 0.11 | 0.44 |
| Gross Receipts Tax on Direct Costs | percent | 6.25 | 6.25 |
| Initial Capital Cost | million $ | 7.10 | 27.54 |
| CAPEX capital expenditure per kWh | $/kWh | 31.68 | 2.93 |
| Cost of Financing | | | |
| Lifetime of facility | years | 30 | 30 |
| Nominal interest rate, R | per year | 0.06 | 0.06 |
| Inflation rate, i | per year | 0.02 | 0.02 |
| Real Interest rate, r (discount rate) | per year | 0.04 | 0.04 |
| Capital Recovery Factor (CRF) | per year | 0.06 | 0.06 |
| Annualized Capital Cost = CRF*Initial Capital Cost | million $ | 0.41 | 1.58 |
| Operation and Maintenance (O&M) Cost | | | |
| Number of employees | - | 2 | 2 |
| Loaded cost of employee per year | Million $/yr | 0.10 | 0.10 |
| Total cost of employees per year | Million $/yr | 0.20 | 0.20 |
| Cost of repairs per year | Million $/yr | 1.0 | 1.0 |
| Annual Operating and Maintenance Cost | Million $ per year | 1.2 | 1.2 |
| Cost of Purchased Electricity | | | |
| Cost of electricity for charging | $/kWh | 0.03 | 0.03 |
| Cost per year to charge for environmental losses | Million $ | 0.04 | 1.56 |
| Cost per year to charge for electricity produced | Million $ | 3.99 | 1.64 |
| Annual Cost of Purchased Electricity | Million $ / yr | 4.03 | 3.2 |